CORE
Metadata, citation and similar papers at core.ac.uk
Provided by Scientific Open-access Literature Archive and Repository

IL NUOVO CIMENTO **41 C** (2018) 97
DOI 10.1393/ncc/i2018-18097-4

COMMUNICATIONS: SIF Congress 2017

Measurements of Higgs boson production cross section and CP violation in the $H \to \tau\tau$ decay channel with the ATLAS detector

A. MURRONE
INFN Milano and Università di Milano, Dipartimento di Fisica - Milano, Italy

received 4 May 2018

Summary. — The $H \to \tau\tau$ decay is an important decay mode of the Higgs as it allows to measure directly the Higgs coupling to fermions. This paper presents the measurement of the $H \to \tau\tau$ cross section performed with the Run 1 dataset (2011–2012) collected by the ATLAS experiment and describes future perspectives for the Run 2 of the LHC, with particular emphasis on the importance of theory uncertainties for this channel. In addition a CP violation measurement in the Vector Boson Fusion production of the Higgs will be shown, that demonstrates how the $H \to \tau\tau$ channel allows to measure the Higgs CP properties as well.

1. – Introduction

The Higgs boson was discovered by ATLAS and CMS Collaborations in July 2012 [1, 2]. All the measurements performed so far have not shown any significant deviation from the Standard Model (SM) expectation. Many of the measurements have been performed in the bosonic decay channels but it is of high importance to confirm the fermions mass generation mechanism by directly measuring the Higgs coupling to fermions. In this sense the $H \to \tau\tau$ decay mode is the most promising channel for its better signal-background separation with respect to the other fermionic decay modes. In addition it can play a role for other Higgs properties measurements such as the measurement of its CP properties. The $H \to \tau\tau$ decay channel has a complex signature as the visible decay products of the τ can be either leptons or hadrons and they are always together with neutrinos. We can identify three subchannels: a channel where both of the two taus have decayed leptonically and the notation $\tau_{\text{lep}}\tau_{\text{lep}}$ will be used in the paper, a channel where one tau has decayed leptonically and the other hadronically with the notation $\tau_{\text{lep}}\tau_{\text{had}}$ and in the end a channel where both the taus have decayed hadronically, with the notation $\tau_{\text{had}}\tau_{\text{had}}$. This paper summarizes the two important results for the $H \to \tau\tau$ cross section [3] and the CP-violation measurements [4] reached with the Run 1 data at $\sqrt{s} = 8\,\text{TeV}$ (2011–2012) collected by the ATLAS experiment corresponding to $20\,\text{fb}^{-1}$. In addition, the perspectives of the current ongoing analyses which are using the

© CERN on behalf of the ATLAS Collaboration
Creative Commons Attribution 4.0 License (http://creativecommons.org/licenses/by/4.0)

data coming from the Run 2 of the LHC will be described, highlighting the importance of systematics, in particular the ones related to the theory.

2. – The ATLAS detector

The ATLAS detector [5] at the LHC covers nearly the entire solid angle around the collision point. The ATLAS coordinates system is right-handed: the z-axis is along the beam direction, the y-axis points upwards from the Earth's surface and the x-axis points towards the center of the LHC ring. The azimuthal angle ϕ runs in the transverse plane around the beam-line. The polar angle θ is measured from beam-axis, but commonly the pseudorapidity is used instead: $\eta = -\ln[\tan\theta/2]$.

The detector consists of an inner tracking detector surrounded by a thin superconducting solenoid, electromagnetic and hadronic calorimeters, and a muon spectrometer incorporating three large superconducting toroid magnets. The inner-detector system (ID) is immersed in a 2 T axial magnetic field and provides charged particle tracking in the range $|\eta| < 2.5$. A high-granularity silicon pixel detector covers the vertex region and typically provides three measurements per track. It is followed by a silicon microstrip tracker, which usually provides four two-dimensional measurement points per track. These silicon detectors are complemented by a transition radiation tracker, which enables radially extended track reconstruction up to $|\eta| < 2.0$. The transition radiation tracker also provides electron identification information based on the fraction of hits above a higher energy-deposit threshold corresponding to transition radiation. The calorimeter system covers the pseudorapidity range $|\eta| < 4.9$. Within the region $|\eta < 3.2$, electromagnetic calorimetry is provided by barrel and endcap high-granularity liquid-argon (LAr) electromagnetic calorimeters, with an additional thin LAr presampler covering $|\eta| < 1.8$, to correct for energy loss in material upstream of the calorimeters. Hadronic calorimetry is provided by a scintillator-tile calorimeter, segmented into three barrel structures within $|\eta| < 1.7$, and two LAr hadronic endcap calorimeters. A muon spectrometer (MS) comprises separate trigger and high-precision tracking chambers measuring the deflection of muons in a magnetic field generated by superconducting air-core toroids. The precision chamber system covers the region $|\eta| < 2.7$ with three layers of monitored drift tubes, complemented by cathode strip chambers in the forward region, where the background is highest. The muon trigger system covers the range $|\eta| < 2.4$ with resistive-plate chambers in the barrel, and thin-gap chambers in the endcap regions.

3. – Cross section measurement with the Run 1 dataset

3˙1. *Analysis description.* – The $H \to \tau\tau$ analysis is subdivided in three subchannels: $\tau_{\rm lep}\tau_{\rm lep}$, where two isolated leptons of opposite charge are required, $\tau_{\rm lep}\tau_{\rm had}$, where exactly one isolated lepton and one hadronic decayed tau of opposite charge are required and finally $\tau_{\rm had}\tau_{\rm had}$, where two isolated hadronic decayed tau are required.

For each channel two exclusive analysis categories are defined: the VBF and the Boosted category. The VBF category is sensitive to events produced through vector boson fusion (VBF) and it is characterized by two high $p_{\rm T}$ jets well separated in rapidity while the Boosted contains events that fail VBF selection and have an high $p_{\rm T}$ Higgs boson candidate and it is dominated by events produced via gluon-gluon fusion (ggF). In table I the VBF and Boosted selections are shown for each channel, where $m_{\tau\tau}^{\rm vis}$ is the invariant mass of the visible tau decay products and the Higgs transverse momentum, $p_{\rm T}^{\rm H}$, is reconstructed from the vector sum of the missing transverse momentum and

TABLE I. – *VBF and Boosted selections for each channel:* $\tau_{\rm lep}\tau_{\rm lep}$, $\tau_{\rm lep}\tau_{\rm had}$, $\tau_{\rm had}\tau_{\rm had}$.

Channel	VBF
$\tau_{\rm lep}\tau_{\rm lep}$	At least two jets with $p_T^{j_1} > 40\,\text{GeV}$ and $p_T^{j_2} > 30\,\text{GeV}$ $\Delta\eta(j_1, j_2) > 2.2$
$\tau_{\rm lep}\tau_{\rm had}$	At least two jets with $p_T^{j_1} > 50\,\text{GeV}$ and $p_T^{j_2} > 30\,\text{GeV}$ $\Delta\eta(j_1, j_2) > 3.0$ $m_{\tau\tau}^{\rm vis} > 40\,\text{GeV}$
$\tau_{\rm had}\tau_{\rm had}$	At least two jets with $p_T^{j_1} > 50\,\text{GeV}$ and $p_T^{j_2} > 30\,\text{GeV}$ $p_{\rm T}^{j_2} > 35\,\text{GeV}$ for jets with $\lvert\eta\rvert > 2.4$ $\Delta\eta(j_1, j_2) > 2.0$
Channel	Boosted
$\tau_{\rm lep}\tau_{\rm lep}$ All	At least one jet with $p_{\rm T} > 40\,\text{GeV}$ Failing the VBF selection $p_{\rm T}^{\rm H} > 100\,\text{GeV}$

the transverse momentum of the visible tau decay products.

Once the events are selected in these two categories, a multivariate analysis is performed for separating signal from background. The multivariate technique uses the Boosted Decision trees (BDT) [6] algorithm to extract the Higgs signal in each category. Among the variables used for the BDT the most discriminating ones are the reconstruced mass of the Higgs $m_{\tau\tau}^{MMC}$ [7], $\Delta R(\tau_1, \tau_2)$ and $\Delta\eta(j_1, j_2)$. Figure 1 shows the output of the BDT in the $\tau_{\rm lep}\tau_{\rm lep}$ channel for VBF (a) and Boosted (b) category.

For the modelling of backgrounds dedicated control regions are used ($Z \to \tau\tau$, top, W-enriched, etc....) and the estimation is done using either Monte Carlo or data-driven techniques (like for the $Z \to \tau\tau$ irreducible background).

Finally, a maximum-likelihood fit is performed in all the signal regions for extracting the signal strenght μ, defined as the ratio of the measured signal yield over the Standard Model expectation. The control regions are also included in the fit as they provide the normalization of the backgrounds. The impact of the systematic uncertainties on the signal and background is described by the nuisance parameters $\vec{\theta}$ and the final test statistic is constructing according to the profile likelihood ratio

$$q_\mu = -2\ln[\mathcal{L}(\mu, \hat{\hat{\vec{\theta}}})]/\mathcal{L}(\hat{\mu}, \hat{\vec{\theta}}),$$

where $\hat{\mu}$ and $\hat{\vec{\theta}}$ are the parameters that maximise the likelihood and the $\hat{\hat{\vec{\theta}}}$ are the nuisance parameters that maximise the likelihood for a given μ. This test statistic shows the compatibility of the data with the background only hypothesis.

3˙2. *Results*. – The signal strength obtained with the Run 1 data corresponding to $20\,\text{fb}^{-1}$ of integrated luminosity and combining all the results for each channel and category is $\mu = 1.43^{+0.27}_{-0.26}(\text{stat})\ ^{+0.32}_{-0.25}\ (\text{syst})\ \pm 0.09\ (\text{theory syst.})$ with an observed (expected) significance of $4.5\sigma(3.4\sigma)$ [3]. This result has proved the evidence for the decay of the Higgs boson into pairs of tau leptons and combined with the CMS Run 1 measurement it has lead to the discovery of the Higgs decay to taus leptons: the measured signal strength is $\mu = 1.12 \pm^{+0.25}_{-0.23}$ with an observed significance of 5.5σ [8].

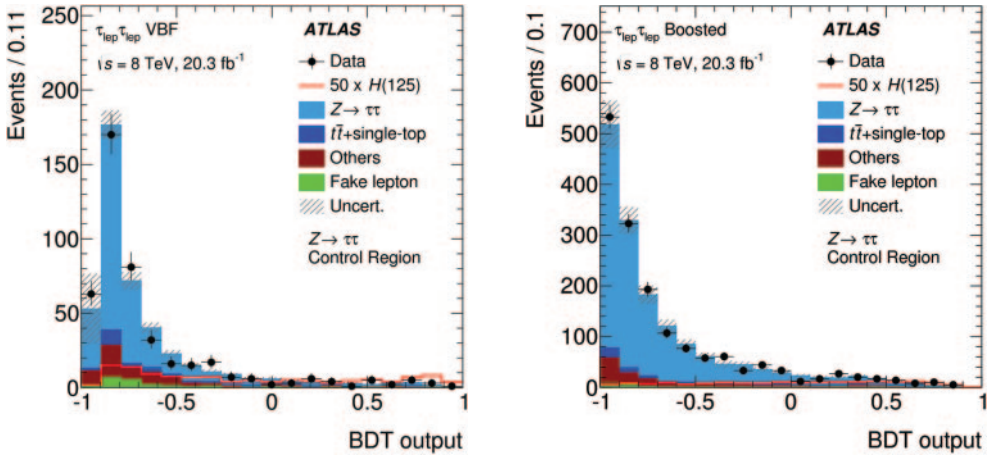

(a) (b)

Fig. 1. – BDT output score in $\tau_{lep}\tau_{lep}$ channel for VBF (a) and Boosted (b) category.

4. – CP-violation measurement

4˙1. *Introduction.* – It is highly important to establish whether the Higgs boson discovered by the ATLAS and CMS experiments is really the particle predicted by the Standard Model (SM) and in order to verify it one has to measure its properties. The analysis performed in the $H \to \tau\tau$ channel with the Run 1 data has looked in particular for *CP* violation in the Higgs sector. *CP* violation is one of the three Sakharov conditions [9] for explaining the baryon asymmetry in the universe. The magnitude of *CP* violation provided in the SM by the Cabibbo-Kobayashi-Maskava matrix [10, 11] is not sufficient to explain the observed value of baryon asymmetry, therefore new sources of *CP* violation not predicted by the SM should be introduced. The Higgs sector is an interesting sector where to look as it has been recently discovered and still need to be explored entirely. The presence of *CP*-violation would be an unequivocal sign of new physics Beyond the Standard Model (BSM).

The measurement performed is the first direct test of *CP* invariance in the Higgs boson production via Vector Boson Fusion (VBF). In principle the method is applicable to any Higgs decay but the $H \to \tau\tau$ allows to select a sizeable amount of VBF events.

Based on the effective Lagrangian framework, the most general Lorentz-invariant tensor structure of the vertex where the Higgs couples to two electroweak vector bosons can be written as [12]

$$(1)\quad T^{\mu\nu}(p_1,p_2) = a_1(p_1,p_2)g^{\mu\nu} + a_2(p_1,p_2)[p_1\cdot p_2 g^{\mu\nu} - p_2^{\mu}p_1^{\nu}] + a_3(p_1,p_2)\epsilon^{\mu\nu\rho\sigma}p_{1\rho}p_{2\sigma},$$

where the a_i are momentum dependent form factors and the p_i denote the momenta of the electroweak gauge bosons. In the SM at tree level only the term with a_1 holds and $a_1 = \frac{2m_V^2}{v}$, where $V = Z, W, \gamma$. If we consider a *CP*-odd perturbation to the SM term, this yields $a_1, a_3 \neq 0$, $a_2 = 0$. The a_3 form factor can be related to two parameters called

$\tilde{d}$ and $\tilde{d}_B$ following the relations

$$a_3^{HZZ} = \frac{2e}{M_W \sin\theta_W}(\tilde{d}\cos^2\theta_W + \tilde{d}_B \sin^2\theta_W), \tag{2}$$

$$a_3^{HWW} = \frac{2e}{M_W \sin\theta_W}\tilde{d}, \tag{3}$$

$$a_3^{HZ\gamma} = \frac{2e}{M_W}(\cos\theta_W(\tilde{d} - \tilde{d}_B),$$

$$a_3^{H\gamma\gamma} = \frac{2e}{M_W \sin\theta_W}(\tilde{d}\sin^2\theta_W + \tilde{d}_B \cos^2\theta_W),$$

where e is the elementary charge, M_W is the mass of the W boson and θ_W is the Weinberg angle.

The parameters $\tilde{d}$ and $\tilde{d}_B$ can be directly measured using a discriminant variable which is sensitive to the presence of *CP*-odd contribution. In this analysis the constraint $\tilde{d} = \tilde{d}_B$ which preserves custodial symmetry, is assumed. With this assumption a generic matrix-element with a *CP*-odd term can be written as

$$\mathcal{M}_{non-SM} = \mathcal{M}_{SM} + \tilde{d}\mathcal{M}_{CP-odd} \tag{4}$$

and then the squared matrix element as

$$|\mathcal{M}_{non-SM}|^2 = |\mathcal{M}_{SM}|^2 + \tilde{d} \cdot 2\mathcal{R}](\mathcal{M}^*_{SM}\mathcal{M}_{CP-odd}) + \tilde{d}^2 \cdot |\mathcal{M}_{CP-odd}|^2. \tag{5}$$

From the squared matrix element it is possible to define the first order Optimal Observable [13-15] as follows:

$$O_1 = \frac{2\mathcal{R}](\mathcal{M}^*_{SM}\mathcal{M}_{CP-odd})}{|\mathcal{M}_{SM}|^2}. \tag{6}$$

The first order Optimal Observable allows to distinguish between a SM and a BSM scenario, indeed it has $\langle O \rangle = 0$ and it is symmetric if we are in the case of SM while it has $\langle O \rangle \neq 0$ and it is not symmetric if a *CP*-odd contribution is present. The Optimal Observable is reconstructed using the four-momenta of the two leading jets and the Higgs and the two Bjorken x from the initial state partons. A distribution of the Optimal Observable at truth-level for the SM and different BSM scenarios is shown in fig. 2.

4˙2. *Analysis description.* – The analysis has been performed on the dataset collected by ATLAS during Run 1 corresponding to $20\,\text{fb}^{-1}$ of integrated luminosity. Since the analysis is essentially based on the $H \to \tau\tau$ coupling analysis, most of the techniques are described in sect. **3**. The first main difference is that here we are interested only in VBF events, therefore all the other production modes of the Higgs are considered as backgrounds. The same preselection and selections of the coupling analysis are applied and for enhancing the signal (VBF events) to background separation a BDT is used in the VBF region identified by the selection in table I. The Optimal Observable is then used in every signal region for measuring $\tilde{d}$ and its modelling is also validated for various backgrounds processes in dedicated control regions (Top, Low BDT and $Z \to ll$ in the $\tau_{\text{lep}}\tau_{\text{lep}}$ channel). In fig. 3 an example of Optimal Observable behaviour in a signal and a control region is shown.

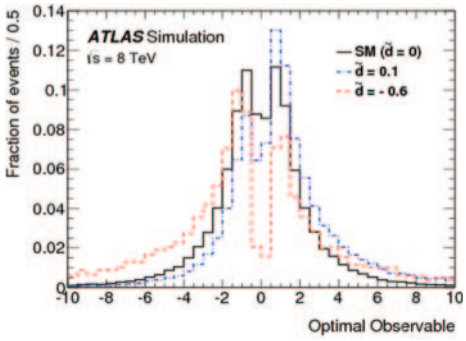

Fig. 2. – Distribution of the Optimal Observable at generator level at leading order. The continuous line is the SM while the dotted lines are for different values of $\tilde{d}$.

A maximum likelihood fit is performed on the Optimal Observable in each signal region and using constraints to the backgrounds coming from control regions. The likelihood is evaluated for different $\tilde{d}$ hypotheses using the corresponding signal sample but since the production of these signal samples is CPU and time consuming a reweighting technique has been devoleped [16] which allows to obtain a BSM sample starting from the SM one.

4˙3. *Results*. – The $\tilde{d}$ parameter has been excluded in the regions $\tilde{d} < -0.11$ and $\tilde{d} > 0.05$ at 68% C.L. [4]. The distribution of the negative log-likelihood is shown in fig. 4.

The technique presented here is interesting and innovative and it allows to improve other results obtained in the HWW and HZZ decays in ATLAS [17]. The statistic of Run 1 is limited but this measurement is supposed to be improved significantly with the Run 2 dataset (expected to be $100\,\text{fb}^{-1}$ of integrated luminosity at the end of the run) and in addition it will be possible to make a combined measurement with other Higgs boson decay channels.

5. – Cross section measurement with the Run 2 dataset

For the $H \to \tau\tau$ channel there is currently an ongoing analysis which is performing a cross section measurement of the Higgs boson production using data coming from the Run 2 of the LHC. The integrated luminosity at the end of the run should be of $100\,\text{fb}^{-1}$, as planned by the LHC official schedule [18], 5 times higher than the integrated luminosity reached in the Run 1, and the center of mass energy has been brought from 8 TeV to 13 TeV, therefore the statistics will be improved significantly. For instance we can consider the two main Higgs production processes at the LHC, ggF and VBF, their cross section increases from $\sim 21\,\text{pb}$ to $\sim 48\,\text{pb}$ for ggF and from $\sim 1.6\,\text{pb}$ to $\sim 3.7\,\text{pb}$ for VBF, thus the number of events, before trigger and selection, which is proportional to the integrated luminosity times the cross section should be ~ 11 higher than in Run 1 for ggF and ~ 12 higher than in Run 1 for VBF. With the increase of statistics the statistical uncertainty will be less relevant compared to the systematics uncertainties. A crucial issue of the Run 2 analysis will be then the evaluation and monitoring of the systematic uncertainties.

As an example CMS has published a paper for $H \to \tau\tau$ cross section measurement with the Run 2 data collected by the detector in 2015–2016 [19] and the measured signal

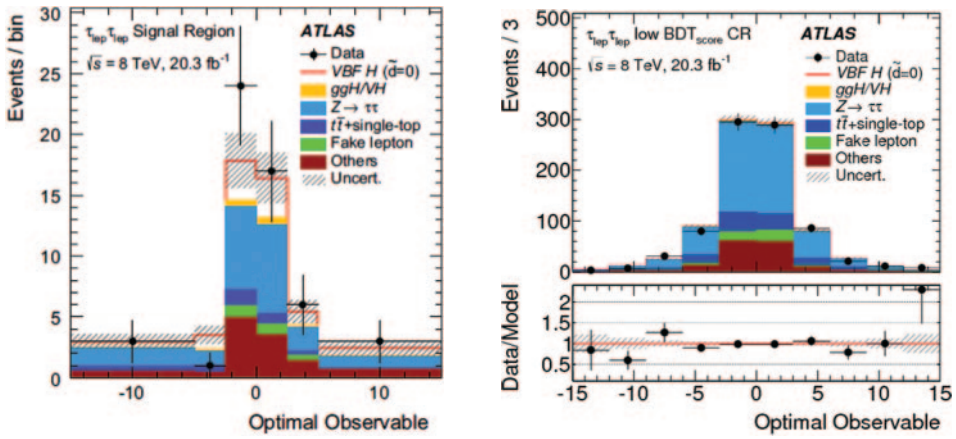

(a) (b)

Fig. 3. – Optimal Observable distribution in the signal region (a) and in the low BDT control region (b) for the $\tau_{\rm lep}\tau_{\rm lep}$ channel.

strength is $\mu = 1.09^{+0.15}_{-0.15}$ (stat) $^{+0.16}_{-0.15}$ (syst) $^{+0.10}_{-0.08}$ (theo) $^{+0.13}_{-0.12}$ (bin by bin) where the separate contributions for the errors are quoted. From this result we can see that the systematic uncertainty is comparable to the statistical one and on top of that the contribution of the theoretical systematics uncertainties is relevant. The next section explains how the theory uncertainties are treated in the $H \to \tau\tau$ ATLAS analysis.

5˙1. *Theory uncertainties.* – The theoretical uncertainties are related to the Higgs production mode, in particular they are not negligible for ggF and VBF, the two main production processes at the LHC and the ones to which the $H \to \tau\tau$ analysis is sensitive. We can identify three main sources of theory uncertainties: QCD scale, parton shower and parton distribution functions.

The QCD scale uncertainties are due to the truncation of the perturbative series and this uncertainty takes into account the missing higher order QCD corrections. In the case of VBF process varying the renormalization and factorization scales gives a very good estimate of the size of the uncertainty while in the case of ggF a trivial scale variation is not sufficient [20]. In the latter case the problem is due to experimental cuts imposed by the analysis which identifies exclusive regions according to the number of final-state jets and this is implicitly done in the VBF and Boosted signal region selections in the $H \to \tau\tau$. Therefore the QCD scale variation for ggF has been evaluated using specific techniques which take into account these effects called Jet Bin Migration.

Another important origin of theory uncertainties is the parton shower model. The parton shower is responsible for the modelling of the process from the hard scattering to low energies where the perturbative QCD breaks down. Here there are a lot of sources of uncertainties that are very difficult to disentagle, from the missing higher order QCD corrections to model of the showering and the hadronization process. The most conservative way to evaluate this uncertainty is to look at the differences between HERWIG [21] and PYTHIA [22] the two main Monte Carlo programs for parton shower. On top of that ATLAS has developed some tunes [23, 24], based on Pythia, that allow to vary some specific parameter of the shower.

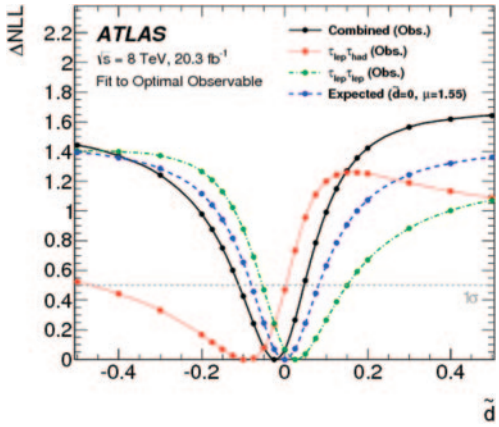

Fig. 4. – Observed and expected ΔNLL curve as a function of the $\tilde{d}$ values. The markers indicate the points where an evaluation was performed and the lines are only meant to guide the eye.

TABLE II. – *Total cross section uncertainties provided by the LHCHXSWG and calculated at N^3LO for the ggH process while at NNLO QCD + NLO EWK for VBF.*

Process	+QCD scale	−QCD scale	±(PDF + α_s)
ggH (N^3LO)	+4.6%	−6.7%	±3.2%
VBF (NNLO QCD + NLO EWK)	+0.4%	−0.3%	±2.1%

The third source are the Parton Distribution Functions (PDF): their distributions are described by the DGLAP equations [25] but the initial values are obtained by fitting to experimental data. For this reason the various available PDF sets use different data and parametrization and they have some internal weights useful for the evaluation of these uncertainties. The PDF sets used for the evaluation of this uncertainty in the $H \to \tau\tau$ analysis are: MSTW2008 [26], CT10 [27], NNNPDF 2.3 [28].

The uncertainties on the total cross sections are provided by the LHC Higgs Cross Section Working Group (LHCHXSWG) [29] and they are shown in table II.

In addition specific acceptance uncertainties have been calculated for the $H \to \tau\tau$ analysis and preliminary evaluations are summarized in table III. The calculations have been performed using the methods described above and using simulations at generator level. All the additional uncertainties are therefore calculated as acceptance uncertainties apart from the QCD scale variation for ggF. For evaluating the QCD scale variation uncertainty for ggF, the Stewart-Tackmann procedure has been used [20] and the MCFM Monte Carlo program [30], which is able to generate fixed order predictions, has been employed. This Monte Carlo is however able to calculate only cross sections and not to generate events, therefore the uncertainty has been computed only for the cross section.

As shown by table III the largest uncertainty for the acceptance is coming from the comparison between Herwig and Pythia. This could in principle overestimate a bit the uncertainty but it is still the most conservative way to calculate it. The plot in fig. 5 shows the differences in the modelling of the mass of the first two leading jets between Herwig and Pythia, already before any specific selections of the analysis is applied. The

TABLE III. – *Summarized results for theory uncertainties in the $H \to \tau\tau$ analysis. The QCD scale uncertainty for the ggF process is on the cross section as the MCFM Monte Carlo, which is able to calculate only cross section and not to generate events, was used.*

	VBF	ggF
QCD scale	∼1%	∼25%(on the cross section)
Parton shower - Tunes variations	∼2%	∼7%
Parton shower - Herwig/Pythia	∼8%	∼15%
PDF	∼2%	∼2%

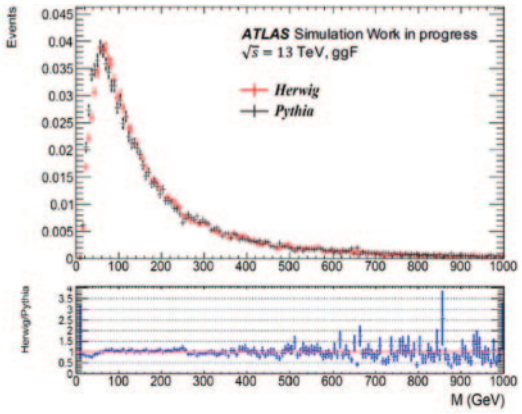

Fig. 5. – Mass of the dijet system modelled in Herwig and Pythia. Discrepancies between the two generators can be better noticed in the ratio plot.

discrepancy reaches about 20% in some bins and it is reliable on the different algorithms used by the two Monte Carlo both for the showering, which is momentum ordered for Pythia and angular ordered for Herwig and for the hadronization process (Lund string model for Pythia and cluster model for Herwig [31]).

6. – Conclusions

The $H \to \tau\tau$ is a promising channel which can allow to measure the Higgs coupling to fermions and the Higgs boson properties. The signal strength has already been measured using the Run 1 data and its measured value is $\mu = 1.43^{+0.43}_{-0.37}$ with significance 4.5σ and compatible with the Standard Model expectation within the uncertainties. This result combined with the CMS measurement has lead to the discovery of Higgs decay to pairs of tau leptons, indeed the signal strength resulted is $\mu = 1.12\pm^{+0.25}_{-0.23}$ with an observed significance of 5.5σ. The Run 2 analysis is currently ongoing and the aspect of systematics, in particular systematics related to theory has been highlighted. The largest systematics are about 15% but they will be reduced with new higher order signal sample and the availability of a new release of Herwig.

The $H \to \tau\tau$ can be used for measuring the *CP* properties of the Higgs as well, as demonstrated by the *CP* measurement performed in the Run 1 which has excluded the *CP* violation parameter in the regions $\tilde{d} < -0.11$ and $\tilde{d} > 0.05$ at 68% of C.L. The innovative technique of the Optimal Observable is highly promising and the result can be improved with the statistic of Run 2.

REFERENCES

[1] The ATLAS Collaboration, *Phys. Lett. B*, **716** (2012) 1.
[2] The CMS Collaboration, *Phys. Lett. B*, **716** (2012) 30.
[3] The ATLAS Collaboration, *JHEP*, **04** (2015) 117.
[4] The ATLAS Collaboration, *Eur. Phys. J. C*, **76** (2016) 658.
[5] The ATLAS Collaboration, *JINST*, **3** (2008) S08003.
[6] Breiman L., Friedman J., Olshen R. and Stone C., *Classification and Regression Trees* (Chapman & Hall, New York) 1984.
[7] Elagin A. *et al.*, *Nucl. Instrum. Methods A*, **654** (2011) 481.
[8] The ATLAS collaboration, *JHEP*, **08** (2016) 045.
[9] Sakharov A. D., *Zh. Eksp. Teor. Fiz. Pisma*, **5** (1967) 32.
[10] Kobayashi M. and Maskawa T., *Prog. Theor. Phys.*, **49** (1973) 652.
[11] Cabibbo N., *Phys. Rev. Lett.*, **12** (1964) 62.
[12] Hankele V., Klamke G. and Zeppenfeld D., *Phys. Rev. D*, **74** (2006) 095001.
[13] Davier M. *et al.*, *Phys. Lett. B*, **306** (1993) 411.
[14] Diehl M., Nachtmann O. and Nagel F., *Eur. Phys. J. C*, **27** (2003) 375.
[15] Diehl M. and Nachtmann O., *Particles and Fields*, **62** (1994) 397.
[16] Murrone A., *Study of the use of Optimal Observables for the Higgs boson CP determination in the vector boson fusion process* Tesi di Laurea Magistrale, 2015.
[17] The ATLAS Collaboration, *Eur. Phys. J. C*, **75** (2015) 476.
[18] `http://lhc-commissioning.web.cern.ch/lhc-commissioning/schedule/LHC-schedule-update.pdf`.
[19] The CMS Collaboration, arXiv:1708.00373.
[20] Stewart W. Iain and Tackmann J. Frank, *Phys. Rev. D*, **85** (2012) 034011.
[21] Belmm J. *et al.*, arXiv:1310.6877.
[22] Sjstrand T. *et al.*, *Comput. Phys. Commun.*, **191** (2015) 159.
[23] The ATLAS Collaboration, ATL-PHYS-PUB-2014-021.
[24] The ATLAS Collaboration, *JHEP*, **09** (2014) 145.
[25] Altarelli G. and Parisi G., *Nucl.Phys. B*, **126** (1977) 298.
[26] Martin A. D. *et al.*, *Eur. Phys. J. C*, **63** (2009) 189.
[27] Lai H. *et al.*, *Phys. Rev. D*, **82** (2010) 074024.
[28] Ball R. D. *et al.*, *Nucl. Phys. B*, **867** (2013) 244.
[29] LHC Higgs Cross section Working Group, arXiv:1610.07922.
[30] Boughezal R., *Eur. Phys. J. C*, **77** (2017) 7.
[31] Webber B. R., *Int. J. Mod. Phys. A*, **15S1** (2000) 577.